



Natural convection of liquid metal in a vertical annulus with lateral and volumetric heating in the presence of a horizontal magnetic field

S.C. Kakarantzas^a, I.E. Sarris^{b,1}, N.S. Vlachos^{b,*}

^a Physique Statistique et Plasmas, CP 231, Université Libre de Bruxelles, 1050 Brussels, Belgium

^b Department of Mechanical Engineering, University of Thessaly, Athens Avenue, 38334 Volos, Greece

ARTICLE INFO

Article history:

Received 30 August 2010

Received in revised form 23 March 2011

Available online 16 April 2011

Keywords:

Free convection

MHD

Annular cavity

Lateral heating

Volumetric heating

Liquid metals

ABSTRACT

MHD free convection of a liquid metal is studied in a closed vertical annulus in which the upper and bottom walls are adiabatic while the cylindrical walls are kept at different temperatures. The flow is driven by two mechanisms; the temperature difference between the two cylindrical walls and the volumetric heating. A constant horizontal magnetic field is also imposed resisting the fluid motion. The laminar and turbulent regimes of the flow are assessed by performing three-dimensional direct numerical simulations. The results show that in the absence of the magnetic field, turbulent flow is developed in most of the cases, while as the magnetic field increases the flow becomes laminar. The highest temperature is found in the upper-central part of the annular cavity when the fluid is heated volumetrically, resulting in the creation of two convection currents as the hot fluid ascends in the central part and descends close to both colder walls. The Hartmann and Roberts layers developing near the walls normal and parallel to the magnetic field, respectively, are found to be responsible for the loss of axisymmetry of the present flow.

© 2011 Elsevier Ltd. All rights reserved.

1. Introduction

Fusion reactors are most promising devices for the production of non-fossil fuel energy in very large quantities. In the last decades, numerous studies have dealt with the transfer of heat from the fusion reactor core which will be assisted by a liquid metal blanket. In such configurations, the increase of heat transfer and the decrease of the pressure drop along the flow channels is of great importance [1]. This is because very high pressure drops occur in duct and pipe flows under strong magnetic fields. As a consequence, the use of forced convection and more specifically liquid pumping for heat removal may become very expensive. In such situations, heat removal by efficient natural convection may be an economic alternative [2,3].

Various natural convection configurations have been proposed as more appropriate for enhancing heat transfer rates. More specifically, Li et al. [4] and Seriwaza et al. [5] suggested a geometry consisting of two coaxial cylinders where liquid metal is placed

in the annular gap and a non-conductive gas (e.g. Helium) is flowing inside the inner cylinder. With this configuration the MHD effects are reduced significantly as the non-conductive gas can remove the heat without any additional pressure drop due to the magnetic field. Uda et al. [6] presented both experimental and numerical results of natural convection of a liquid metal, in a geometry consisting of a tube and a heater pin placed on the axis of the tube. A transverse magnetic field was applied and the mechanism of heat transfer was studied. The $k-\epsilon$ model was used for the numerical calculations, adapted for MHD natural convection flows. Moreover, Serizawa et al. [5] performed an experiment in a vertical tube using NaK/nitrogen flow and, applying an external transverse magnetic field, they demonstrated that heat transfer was non-axisymmetric. Similar results were found in the numerical study of Li et al. [4] for a liquid metal/gas flow in a vertical annulus under the effect of a transverse magnetic field.

In the present work a similar configuration to that used by Kakarantzas et al. [2,3] was considered where a liquid metal with Prandtl number of 0.0321 was placed between two coaxial vertical cylinders. The outer wall temperature was constant and greater than that of the inner. Internal volumetric heating and an external horizontal magnetic field were applied. The combined natural convection flow due to wall temperature difference and the internal heating is the additional feature studied here in relation to the previous work of Kakarantzas et al. [2].

* Corresponding author. Tel.: +30 24210 74094; fax: +30 24210 74085.

E-mail address: vlachos@mie.uth.gr (N.S. Vlachos).

¹ Present address: Technological & Educational Institute of Athens, Energy Technology Department, Ag. Spyridona 17, 12210 Egaleo, Athens, Greece.

Nomenclature

B_0	magnitude of the external magnetic field ($\text{kg}/(\text{s}^2\text{A})$)
g	gravity acceleration (m/s^2)
$Ha = RB_0 \sqrt{\sigma/\rho\nu}$	Hartmann number
\mathbf{J}	electric current density (A/m^2)
k	fluid thermal conductivity ($\text{W}/\text{m}\cdot\text{K}$)
L	height of the cylinders (m)
Nu_i	local Nusselt number at the inner cylinder
\overline{Nu}_i	azimuthally averaged Nusselt number along the inner cylinder
$\overline{Nu}_{i,tot}$	averaged Nusselt number on the inner cylinder
Nu_o	local Nusselt number at the outer cylinder
\overline{Nu}_o	azimuthally averaged Nusselt number along the outer cylinder
$\overline{Nu}_{o,tot}$	averaged Nusselt number on the outer cylinder
p	fluid pressure (Pa)
$Pr = \nu/\alpha$	Prandtl number
Q	volumetric heating rate (W/m^3)
$R = R_o - R_i$	annular gap (m)
$Ra_e = g\beta\Delta T R^3/\nu\alpha$	external Rayleigh number
$Ra_i = g\beta Q R^5/\nu\kappa\alpha$	internal Rayleigh number
R_i	radius of the inner cylinder (m)

R_o	radius of the outer cylinder (m)
r, z	radial and axial spatial coordinates
$S = Ra_i/Ra_e$	ratio of internal-to-external Rayleigh numbers
t	time (s)
T^*	temperature of the fluid
T_i	temperature of the inner cylinder (K)
T_o	temperature of the outer cylinder (K)
$\Delta T = T_o - T_i$	temperature difference between the cylinders (K)
$T = (T^* - T_i)/\Delta T$	non-dimensional temperature
u_r, u_θ, u_z	radial, tangential, and axial velocity components
\mathbf{v}	velocity vector

Greek letters

α	fluid thermal diffusivity (m^2/s)
β	fluid coefficient of thermal expansion ($1/\text{K}$)
θ	azimuthal angle
ν	fluid kinematic viscosity (m^2/s)
ρ	fluid density (kg/m^3)
σ	fluid electrical conductivity ($\text{s}^3\text{A}^2/\text{m}^2\text{kg}$)
Φ	electrical potential ($\text{m}^2\text{kg}/\text{s}^3\text{A}$)

2. Flow configuration and model description

A vertical annular container, as shown schematically in Fig. 1, was considered with an aspect ratio $L/R = 3$, where L is the height of the cylinders, $R = R_o - R_i$ is the annular gap, and R_o, R_i are the radii of the outer and inner cylinders, respectively, with $R_i = 0.2R$. The top and bottom walls were assumed adiabatic while the outer and inner walls were kept isothermal with the outer wall temperature

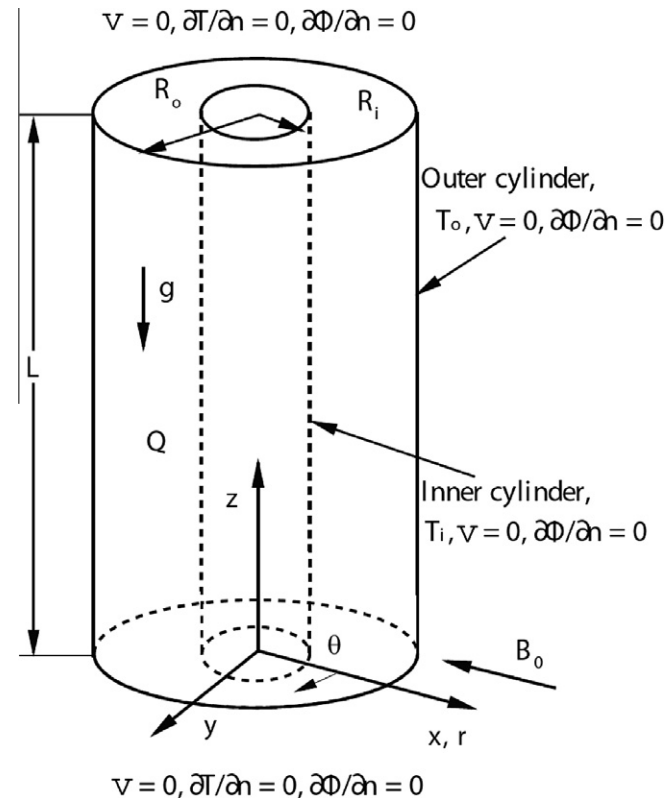


Fig. 1. Flow configuration and boundary conditions.

Table 1

Grid independence test ($Ra_e = 10^5, Ra_i = 0, Ha = 100$).

Grid	$32 \times 32 \times 64$	$64 \times 64 \times 128$	$97 \times 97 \times 176$
Nu	1.843	2.126	2.159
Error	14.6 %	1.5 %	-

T_o greater than that of the inner T_i . The annular container was filled with a low Prandtl number ($Pr = 0.0321$) electrical conducting fluid. Internal volumetric heating and an external horizontal magnetic field were applied. It must be noted that in Fig. 1, Q represents the volumetric heat generation, \mathbf{g} is the gravity acceleration, and \mathbf{B}_0 the constant external magnetic field. All walls were assumed electrically insulated. The aspect ratio of $L/R = 3$ was selected since it corresponds to a fair balance between the actual design needs of the future fusion blanket and the efficiency of the direct numerical simulation method used in the present study.

The governing magnetohydrodynamic equations were non-dimensionalized using as characteristic quantities the annular gap R , the free fall velocity, $u_{ref} = \sqrt{g\beta R\Delta T}$, the pressure, $p_{ref} = \rho u_{ref}^2$, the time, $t_{ref} = R/u_{ref}$, and the electric potential, $\Phi_{ref} = B_0 R u_{ref}$, where, ρ is the density of the fluid and β its volumetric thermal expansion coefficient. The non-dimensional temperature T was calculated from the fluid temperature T^* using the relation $T = (T^* - T_i)/\Delta T$, where $\Delta T = T_o - T_i$ was the temperature difference between the outer and the inner cylindrical walls. Thus, the dimensionless equations become:

$$\nabla \cdot \mathbf{v} = 0, \quad (1)$$

$$\frac{\partial \mathbf{v}}{\partial t} + (\mathbf{v} \cdot \nabla) \mathbf{v} = -\nabla p + \text{Tk} + \left(\frac{Pr}{Ra_e}\right)^{\frac{1}{2}} \nabla^2 \mathbf{v} + Ha^2 \left(\frac{Pr}{Ra_e}\right)^{\frac{1}{2}} (\mathbf{J} \times \mathbf{B}_0), \quad (2)$$

$$\frac{\partial T}{\partial t} + (\mathbf{v} \cdot \nabla) T = \left(\frac{1}{Pr Ra_e}\right)^{\frac{1}{2}} \nabla^2 T + \frac{Ra_i}{(Pr Ra_e)^{\frac{1}{2}}}, \quad (3)$$

$$\nabla^2 \Phi = \nabla \cdot (\mathbf{v} \times \mathbf{B}_0), \quad (4)$$

$$\mathbf{J} = -\nabla \Phi + \mathbf{v} \times \mathbf{B}_0, \quad (5)$$

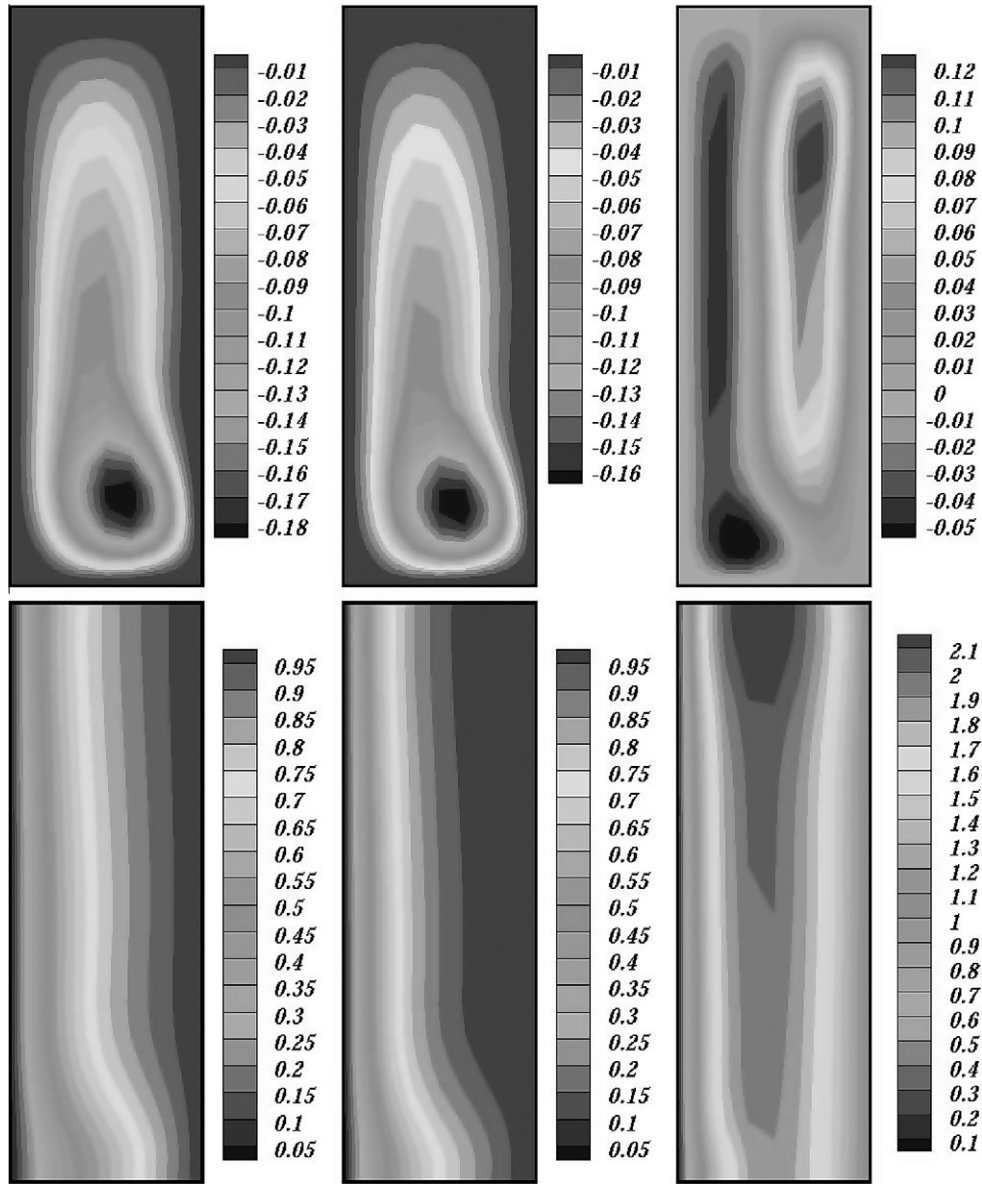


Fig. 2. Distributions of streamfunction (top) and isotherms (bottom) for $Ra_e = 10^3$ and $Ha = 0$: $Ra_i = 0$ (left), $Ra_i = 10^3$ (middle), $Ra_i = 10^4$ (right).

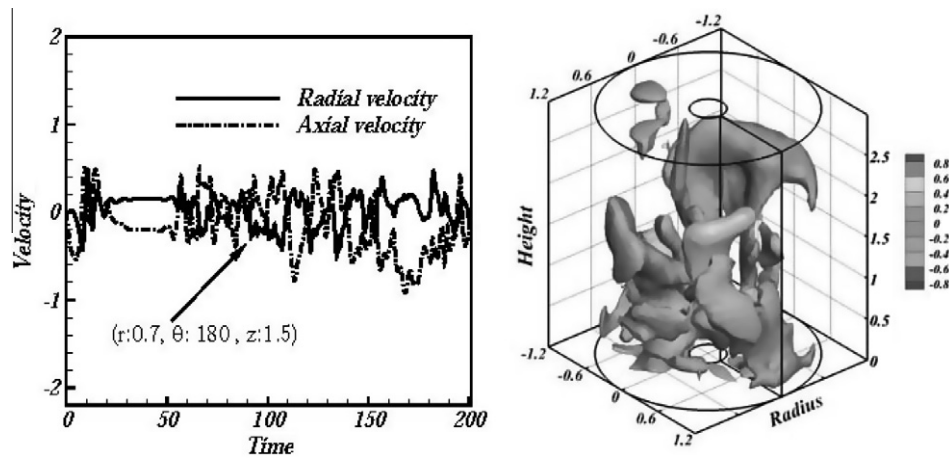


Fig. 3. Time-variation of the axial and radial velocities (left) and 3D distribution of the azimuthal velocity at $t = 200$ (right) for $Ra_e = 10^4$, $Ra_i = 0$, $Ha = 0$.

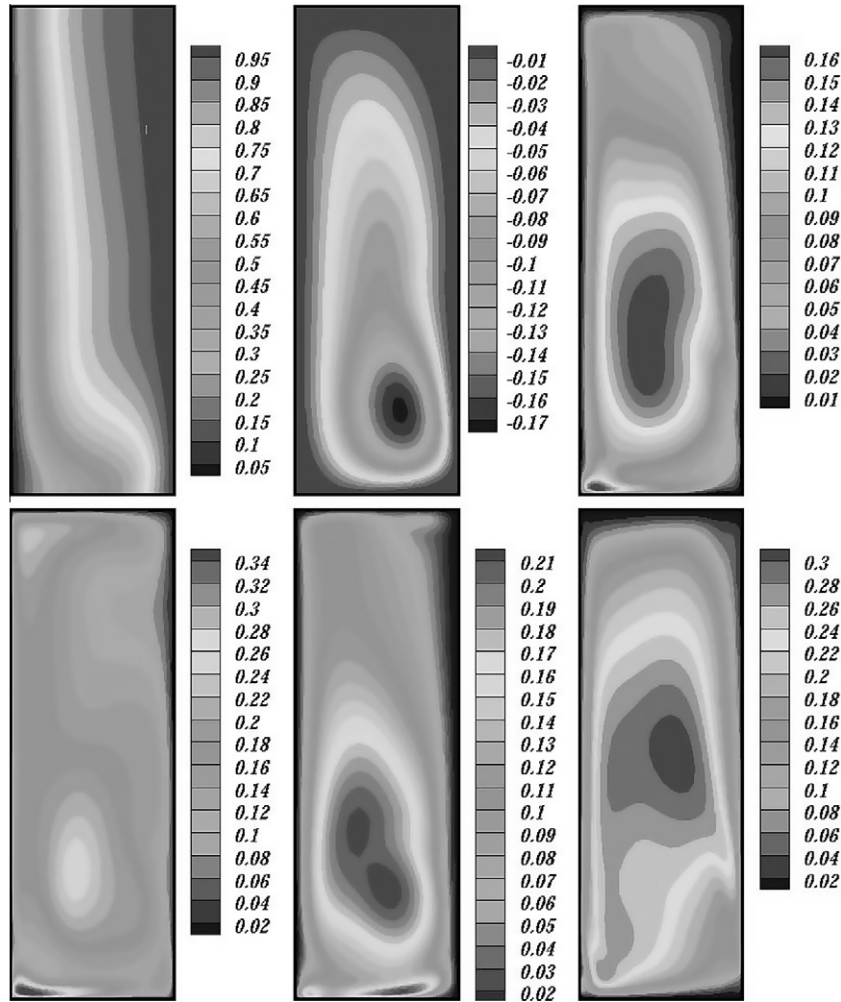


Fig. 4. Azimuthally and time averaged fields of (top left to bottom right) isotherms, streamlines, turbulent kinetic energy and Reynolds stresses $\overline{u'_0 u'_0}$, $\overline{u'_r u'_r}$ and $\overline{u'_z u'_z}$ for $Ra_e = 10^4$, $Ra_i = 0$, $Ha = 0$.

where, \mathbf{k} is the unit vector in the z – direction, Φ the electric potential and \mathbf{J} the electric current. It must be noted that the low magnetic Reynolds number approximation was adopted [7] because, for the present natural convection flow, the magnetic field induced by the fluid motion is assumed to be very small in comparison to the external magnetic field and, thus, the magnetic induction equations need not be solved.

The dimensionless parameters characterizing the present flow are: the external Rayleigh number, $Ra_e = g\beta\Delta TR^3/\nu\alpha$, corresponding to the magnitude of the temperature difference between the external and internal cylinders, the internal Rayleigh number, $Ra_i = g\beta QR^2/\nu k\alpha$, representing the intensity of the volumetric heat generation, and the Hartmann number, $Ha = B_0 R \sqrt{\frac{\sigma}{\rho\nu}}$, expressing the magnitude of the magnetic field, where, ν the kinematic viscosity

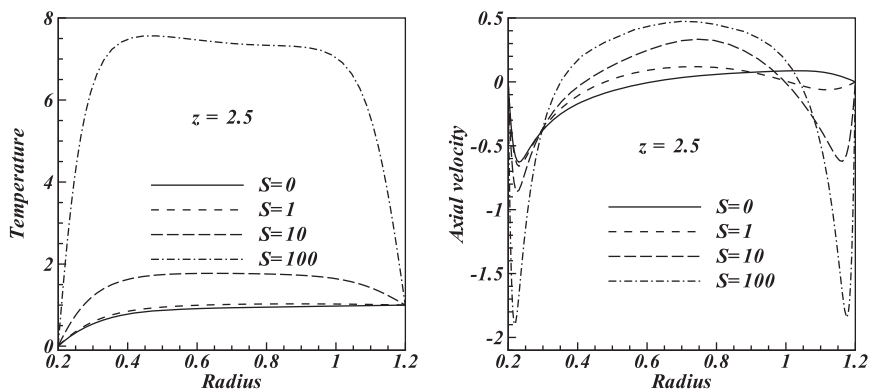


Fig. 5. Radial distribution of the azimuthally and time averaged temperature (left) and axial velocity (right) at $z = 2.5$ for $Ha = 0$, $Ra_e = 10^5$, $S = 0, 1, 10$ and 100 .

of the fluid, k its thermal conductivity coefficient, a its thermal diffusivity coefficient and σ its electrical conductivity. Depending on the combination of these parameters, the flow may become laminar, transitional or turbulent. Also, because the action of the horizontal magnetic field results in non-axisymmetric velocity and temperature fields, three-dimensional computations are needed.

No-slip conditions were assumed on all walls ($u_r = u_\theta = u_z = 0$ for $z = 0, 3$ and $r = 0.2, 1, 2$), and constant temperatures at the inner ($T_i = 0$) and outer ($T_o = 1$) cylindrical walls. Finally, adiabatic conditions were considered at the bottom and top walls ($\partial T / \partial z = 0$ for $z = 0, 3$) and all walls were considered electrically insulated: $\partial \Phi / \partial n = 0$.

The heat transfer characteristics were assessed via the Nusselt number along the inner and outer cylinders calculated from the expressions:

$$Nu_{i,o}(\theta, z) = \ln(R_i/R_o)(r\partial T/\partial r)_{r=R_i,R_o} \quad (6)$$

and the azimuthally-averaged Nusselts numbers calculated from:

$$\overline{Nu}_{i,o} = \frac{1}{2\pi} \int_0^{2\pi} Nu_{i,o}(\theta, z) d\theta, \quad (7)$$

while the average (i.e. averaged axially and azimuthally) Nusselt numbers at the inner and outer walls were calculated, as:

$$\overline{Nu}_{i,o,tot} = \frac{1}{2\pi L} \int_0^{2\pi} \int_0^L Nu_{i,o}(\theta, z) dz d\theta. \quad (8)$$

3. Numerical details

The governing Eqs. (1)–(5) of the present MHD natural convection were discretized using a staggered non-uniform mesh and second-order accurate finite-difference schemes. The resulting system of algebraic equations was solved with a fractional step method where a semi-implicit scheme was used for time integration [8]. The diffusion terms were advanced in time with a Crank-Nicolson method, while the non-linear terms, the buoyancy and Lorentz force terms with a third-order Runge-Kutta method. For a fully resolved direct numerical simulation, the specific features of the present flow and heat transfer problem must be considered. In particular, the increase of Ha results in thinner sidewall and Hartmann layers, while the increase of Ra_e produces thinner boundary layers and smaller Kolmogorov and Batchelor scales. The mesh size for the present direct numerical simulations was selected such that all the flow scales, both in the boundary layers and the bulk flow, could be properly resolved. An estimate for the flow scales was obtained by the analysis proposed by Grötzbach [9] where the appropriate Kolmogorov scale η is a function of Nu number for fluids with $Pr < 1$. Furthermore, for an estimate of the resulting Nu number of each flow case an exponential function of Ra_e and Ha was used according to Aurnou and Olson [10]. In the cases where strong magnetic fields were employed, special care was taken for the resolution of the thinner Hartmann layers, as described by Kakarantzas et al. [2].

Based on the above conditions and depending on the external Rayleigh number Ra_e , the selected computational grids were $(r, \theta, z : 49 \times 49 \times 97)$ for $Ra_e \leq 10^4$ and $(r, \theta, z : 65 \times 65 \times 128)$ for $Ra_e > 10^4$. The adequacy of the grid was assessed by performing grid independence tests of some indicative cases. For example, representative results of the Nusselt number, a quantity most sensitive to the grid, are given in Table 1 for some grids tested. In addition, the present numerical model has been tested successfully by Kakarantzas et al. [2,11] against the numerical results of Sarris et al. [12] and Karcher et al. [13].

4. Results and discussion

Direct numerical simulations were performed for three external Rayleigh numbers ($Ra_e = 10^3, 10^4, 10^5$), six internal Rayleigh numbers ($Ra_i = 0, 10^3, 10^4, 10^5, 10^6, 10^7$) and four Hartmann numbers ($Ha = 0, 25, 50, 100$). Depending on the magnitude of the Hartmann number and the ratio of the internal-to-external Rayleigh numbers,

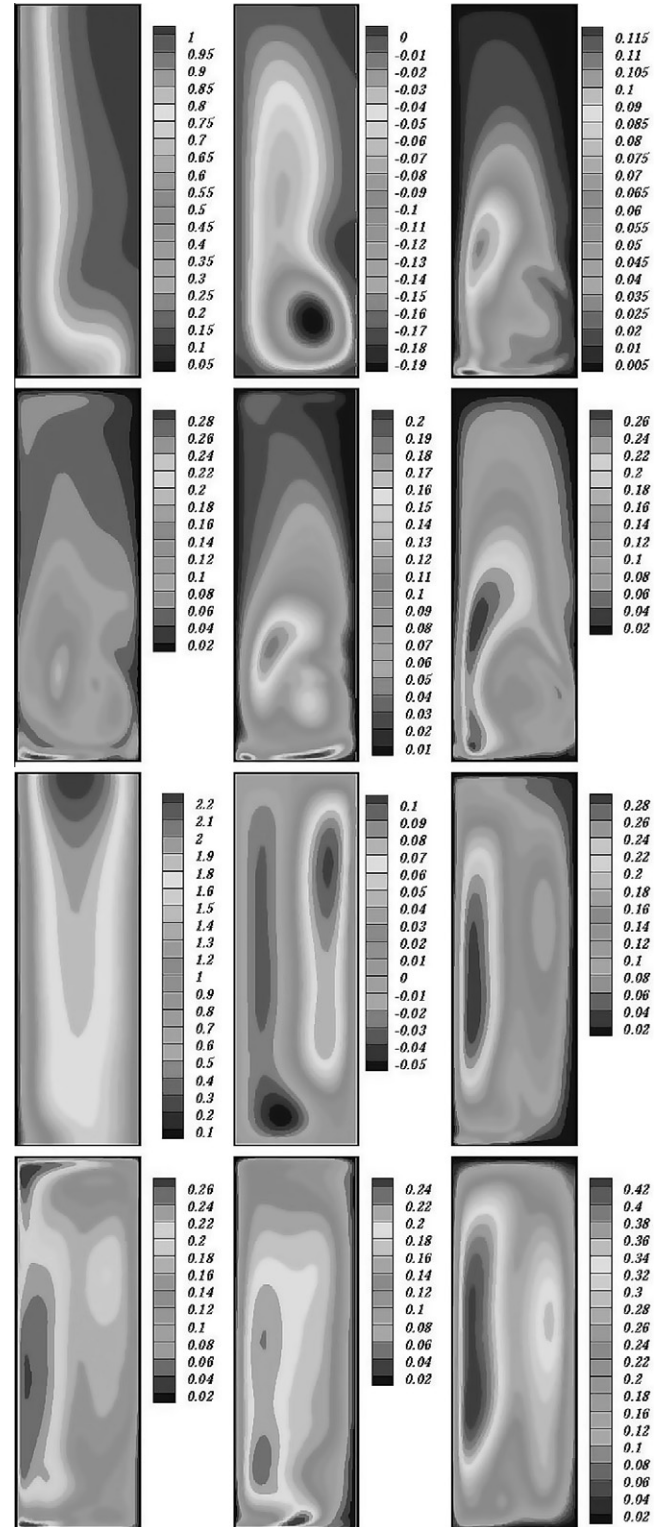


Fig. 6. Azimuthally and time averaged fields of (top left to bottom right) isotherms, streamlines, turbulent kinetic energy and Reynolds stresses $\overline{u'_r u'_r}$, $\overline{u'_\theta u'_\theta}$ and $\overline{u'_z u'_z}$ for $Ha = 0$ and $Ra_e = 10^4$; $Ra_i = 10^4$ (top six plots), $Ra_i = 10^5$ (bottom six plots).

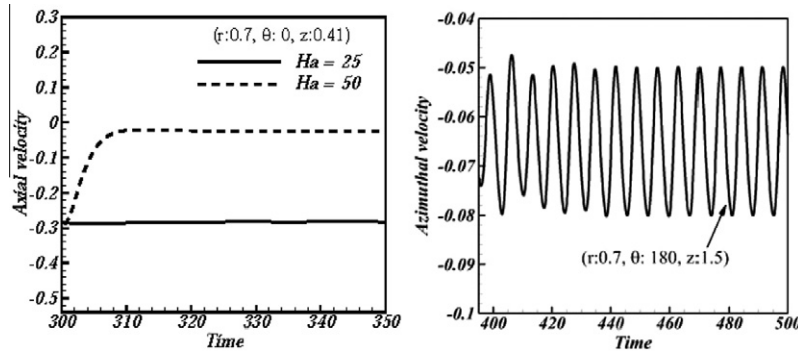


Fig. 7. Time-variation of axial velocity at $(r:0.7, \theta: 0, z:0.41)$ for $Ra_e = 10^4, Ra_i = 0$ and $Ha = 25, 50$ (left) and of azimuthal velocity at $(r: 0.7, \theta: 180, z: 1.5)$ for $Ra_e = 10^4, Ra_i = 10^5, Ha = 25$ (right).

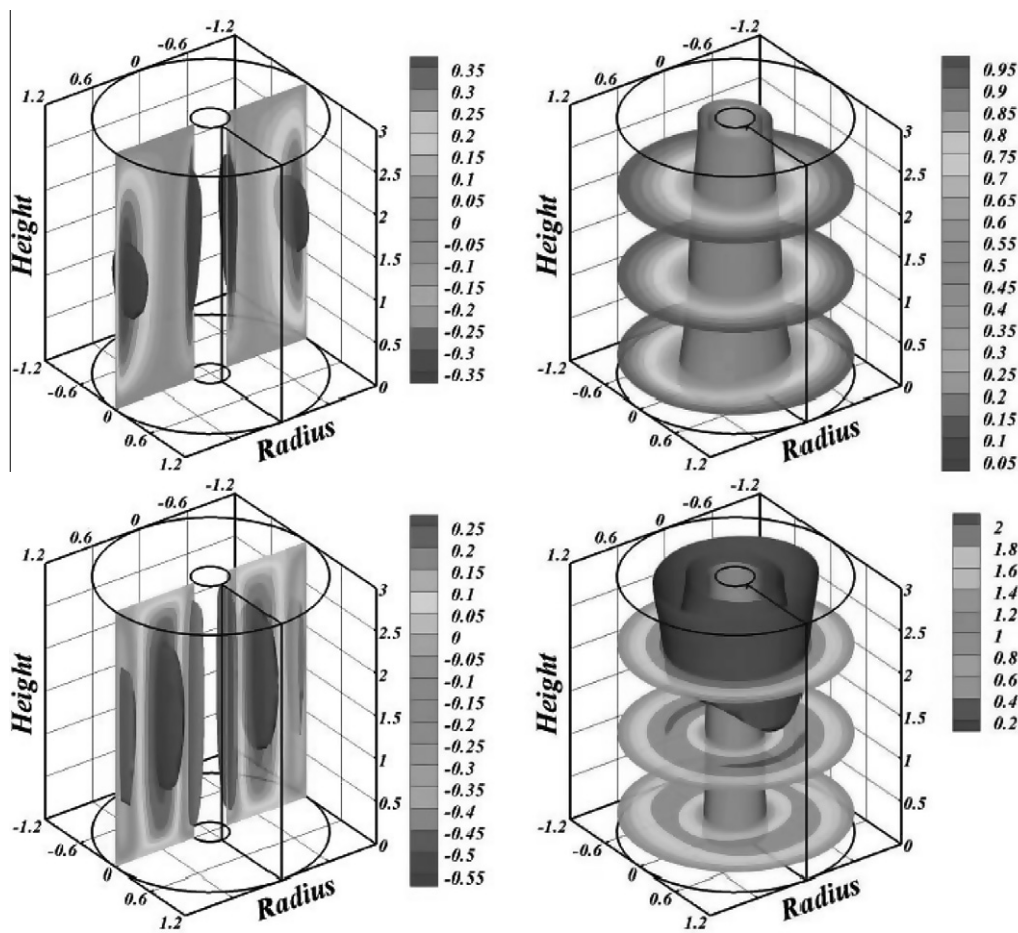


Fig. 8. 3D distribution of axial velocity (left) and temperature (right) for $Ha = 100, Ra_e = 10^4: Ra_i = 0$ (top), $Ra_i = 10^5$ (bottom).

the flow may become laminar, transitional or turbulent. More specifically, in the absence of the magnetic field ($Ha = 0$), turbulent flow develops for $Ra_e \geq 10^4$ for the low Prandtl number ($Pr = 0.0321$) fluid considered here. As Ha increases, transition occurs and, for $Ha > 50$, the disturbances disappear in all cases with the flow becoming laminar.

4.1. Hydrodynamic cases ($Ha = 0$)

In Fig. 2 the main features of the laminar hydrodynamic flow ($Ha = 0$) are presented in terms of streamlines and isotherms for $Ra_e = 10^3$ and $Ra_i = 0, 10^3$ and 10^4 . In all these cases the flow is azi-

mutually symmetric. From the isotherms, it is obvious that when no heat generation is considered, the fluid ascends near the hotter external wall and it descends near the internal wall which is colder. This flow current is depicted by the single flow pattern of the streamfunction plot. The increase of Ra_i alters the flow pattern as the volumetric heating affects the temperature of the fluid and, consequently, its motion. More specifically for $Ra_i = 10^3$, an extended region of hot fluid is formed near the external wall, where its temperature increases due to the volumetric heating and becomes almost equal to the temperature of the external cylindrical wall. Although the temperature field is modified, the single flow pattern still remains. However, as Ra_i increases, the region of the

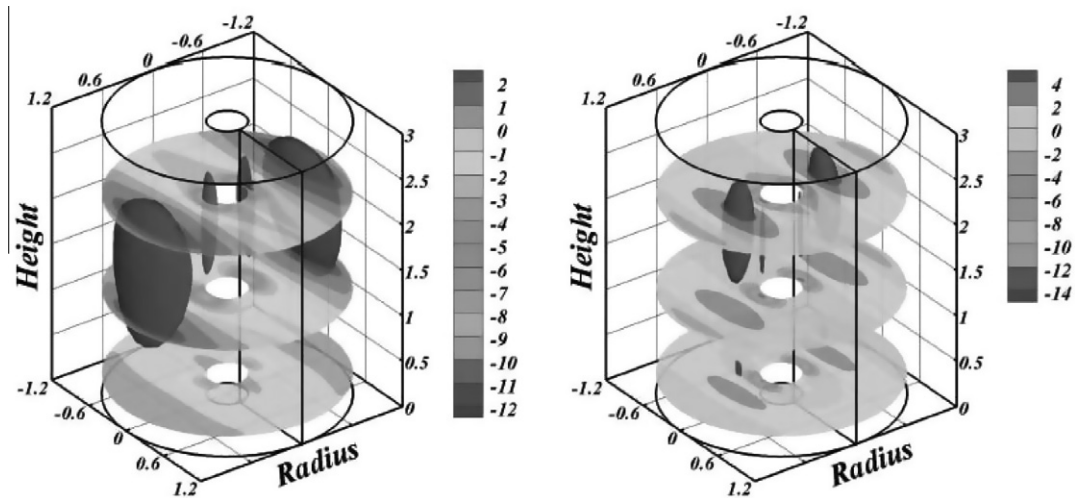


Fig. 9. 3D distribution of axial Lorentz force for $Ha = 50$, $Ra_e = 10^4$: $Ra_i = 0$ (left), $Ra_i = 10^5$ (right).

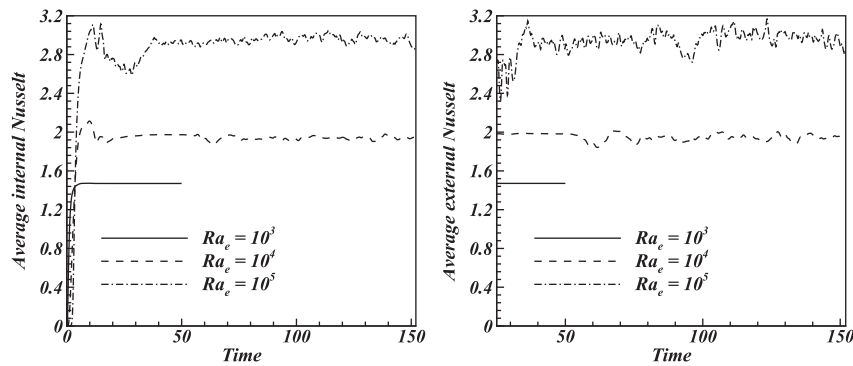


Fig. 10. Time-variation of the average Nusselt number on the internal (left) and external (right) walls for $Ha = 0$, $Ra_i = 0$, $Ra_e = 10^3, 10^4, 10^5$.

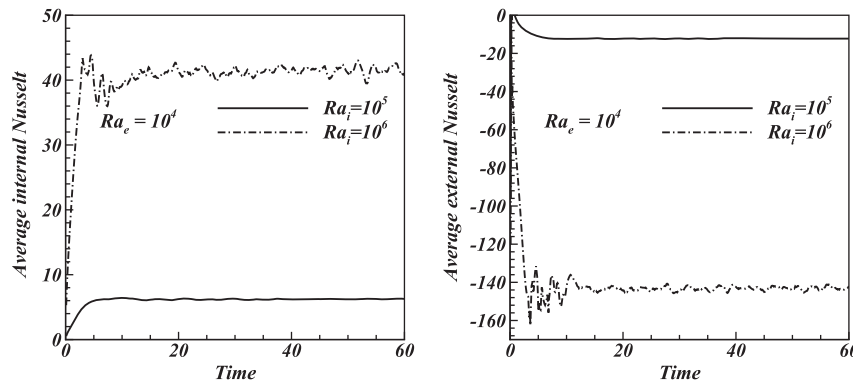


Fig. 11. Time-variation of the average Nusselt number on the internal (left) and the external (right) walls for $Ha = 0$, $Ra_e = 10^4$, $Ra_i = 10^5, 10^6$.

hot fluid moves toward the middle of the annular gap. The local fluid temperature increases further and finally it exceeds that of the external wall. Consequently, the hot ascending fluid at the central part of the domain divides the single flow pattern into a pair of counter-rotating patterns. The fluid descends along the outer and the inner cylindrical walls which are now both at lower temperatures than the bulk fluid. This feature of the volumetric heating has also been observed in other cases of confined natural convection flows, for example [1,14].

As Ra_e increases the flow becomes turbulent in the absence of magnetic field. Fig. 3 shows the temporal variation of the radial and axial velocities at the monitor location ($r : 0.7, \theta : 180, z : 1.5$) and a snapshot at time $t = 200$ of the 3D instantaneous distribution of the azimuthal velocity component for $Ra_e = 10^4$ and $Ra_i = 0$. As it can be observed, the resulting fluid motion is fully disturbed and chaotic and the flow is turbulent.

In Fig. 4 the azimuthally and time averaged distributions of some important turbulent quantities are also presented. From left

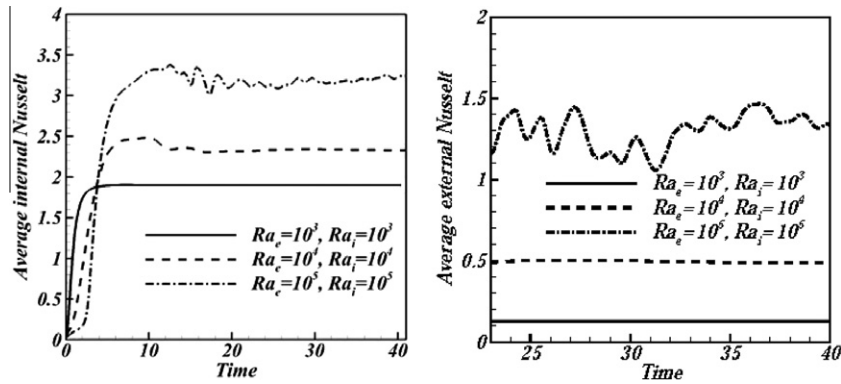


Fig. 12. Time-variation of the average Nusselt on the internal (left) and external (right) walls for $Ha = 0$, $Ra_e = Ra_i = 10^3$, 10^4 and 10^5 .

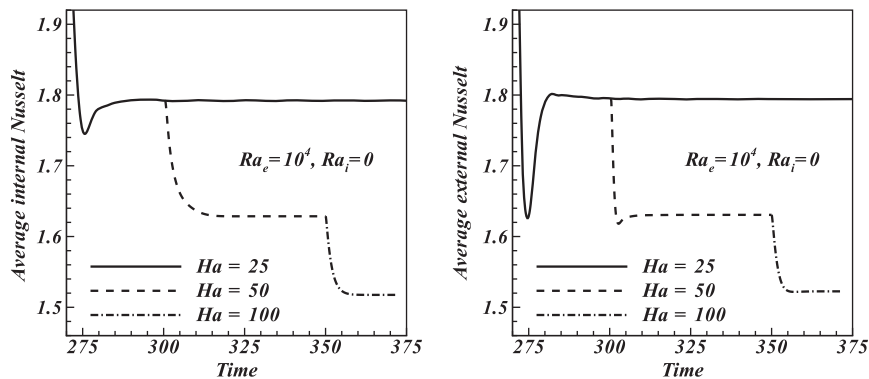


Fig. 13. Time-variation of average Nusselt on the internal (left) and external (right) cylindrical walls for $Ra_e = 10^4$, $Ra_i = 0$, $Ha = 25$, 50 and 100.

to right, these quantities are the isotherms, the streamlines, the turbulent kinetic energy and the Reynolds stresses $\overline{u'_i u'_j}$, $\overline{u'_i u'_r}$ and $\overline{u'_z u'_z}$. It is observed that the Reynolds stress $\overline{u'_i u'_j}$ and $\overline{u'_z u'_z}$ contribute locally the most to turbulence while two highly unstable regions are seen. The first is located near the middle of the annular gap and the second in the corner formed by the internal cylinder with the bottom wall.

When volumetric heating is active, the temperature in the bulk fluid increases resulting to significant changes in the flow pattern. These changes depend on the ratio of the internal-to-external Rayleigh numbers, $S = Ra_i/Ra_e$, as it was also observed for the square cavity reported in Ref. [1]. Similarly to the laminar flow case of Fig. 3, in the present turbulent flow cases and for $S = 1$, the volumetric heating creates a second region (very close to the external wall) where the temperature increases and becomes almost equal to that of the external wall. As S increases further this hot fluid region moves towards the middle of the annular gap and the local fluid temperature increases further. As a result, the temperature at the external wall is no longer the maximum in the domain. Furthermore, the increased temperatures result in the development of steeper temperature gradients close to the cylindrical walls which increase the turbulent fluid motion. The above are confirmed in Fig. 5 where the radial distribution of the azimuthally and time averaged temperature and axial velocity at $z = 2.5$ are presented for $Ha = 0$, $Ra_e = 10^5$ and $S = 0, 1, 10$ and 100.

Concerning the turbulent characteristics of the flow, Fig. 6 shows the azimuthally and time averaged distribution of the isotherms, the streamlines, the turbulent kinetic energy and the Reynolds stresses $\overline{u'_i u'_j}$, $\overline{u'_i u'_r}$ and $\overline{u'_z u'_z}$ for $Ra_e = 10^4$, $S = 1$ and 10. The isotherms and the streamlines confirm the impact of the volumet-

ric heating on the flow pattern, as it is clearly shown by the movement of the temperature maximum, and by the creation of two strong convection currents for $S = 10$. In addition, the distribution of the turbulent kinetic energy for $S = 1$ indicates that two highly unstable regions are formed as in the case without internal heating presented, for example, in Fig. 4. The first region appears close to the internal cylinder and the second in the corner of the internal cylinder and the bottom wall. For $S = 10$ the most unstable area is near the internal cylinder, at its mid height. It may also be concluded that for $Ra_i = 10^4$ (i.e. $S = 1$), all three Reynolds stresses, $\overline{u'_i u'_j}$, contribute almost equally to turbulence, while for $Ra_i = 10^5$ (or $S = 10$) the contribution of $\overline{u'_z u'_z}$ is clearly larger.

4.2. Magnetohydrodynamic cases ($Ha > 0$)

The presence of the magnetic field retards the fluid and progressively causes a transition to laminar flow, while for high enough Hartmann numbers the flow becomes clearly laminar. This is confirmed in Fig. 7 which shows the time-variation of the axial velocity at position ($r : 0.7$, $\theta : 0$, $z : 0.41$) for $Ra_e = 10^4$, $Ra_i = 0$, $Ha = 25$, 50, and of the azimuthal velocity at ($r : 0.7$, $\theta : 180$, $z : 1.5$) for $Ra_e = 10^4$, $Ra_i = 10^5$, $Ha = 25$. An oscillatory behaviour of u_θ is observed in the case of $Ra_i = 10^5$. Furthermore, the magnetic field causes the loss of flow axisymmetry and the formation of wakes near the cylindrical walls that are parallel to its direction. This is due to the fact that Hartmann and side (Roberts) layers are developing near the walls normal and parallel to it, respectively. The flow is retarded more in both layers but inside the Hartmann layers the reduction is larger than in the side layers, see Kakarantzas et al. [2] and Todd et al. [15].

It is known that the thicknesses of the Hartmann and Roberts layers are, in general, proportional to Ha^{-1} and Ha^{-2} , respectively (see Ref. [16] for details). However, in the special case of cylindrical domains with a horizontal magnetic field, the thickness of the Hartmann layer depends on the azimuthal angle θ and it is of the order $(Ha \cos \theta)^{-1}$, see [17–19], while wider Roberts layers are formed [20]. Consequently, wakes are created and the flow loses its axisymmetry. This is shown in Fig. 8 where the three-dimensional distributions of the axial velocity and temperature of the fluid are depicted at $Ha = 100$ for $Ra_e = 10^4$ and $S = 0, 10$.

The impact of the Hartmann and Roberts layers on the flow is expressed via the Lorentz force which is always resisting the fluid motion and it is stronger in regions of higher velocities. This is shown in Fig. 9 where for $Ra_e = 10^4$ and $Ha = 50$ the distribution of the axial component of the Lorentz force is presented for $S = 0$ and 10. It is observed that the values of the Lorentz force are higher in the directions $\theta = 90^\circ$ and 270° (i.e. inside the Roberts layers) where the fluid velocities are also higher.

4.3. Heat transfer

The important problem of heat transfer from the cylindrical walls is studied here via the distribution of the Nusselt number

for a range of flow parameters. The present results confirm the known fact that for the hydrodynamic case and without heat sources, when the external Rayleigh number increases, the average Nusselt number also increases. This is confirmed by the results of Fig. 10 where the time-variation of the average Nusselt number on the internal and the external cylindrical walls for the hydrodynamic cases ($Ha = 0$) and without volumetric heating ($S = 0$), and for $Ra_e = 10^3, 10^4$ and 10^5 is presented.

When volumetric heating is present and for $S > 1$, the increase of the internal Rayleigh number results in the increase of heat transfer. This is observed in Fig. 11 where the time-variation of the average Nusselt number on the internal and the external cylinders is shown for $Ha = 0$, $Ra_e = 10^4$ and $Ra_i = 10^5, 10^6$ (i.e. $S = 10, 100$). It is found that the Nusselt number and, thus, the heat transfer rates are significantly higher at the outer (hotter) wall. Here it must be noted that the observed negative values of the external Nusselt number are due to the movement of the temperature maximum from the outer wall to the bulk fluid. In such cases, the outer wall absorbs the heat transfer from the bulk higher temperature fluid and that is why the values of the Nusselt number are becoming negative. Analogous results can also be found in [3,14].

In the case of $S = 1$, it appears that the heat transfer mechanism is different. More specifically, the average Nusselt number

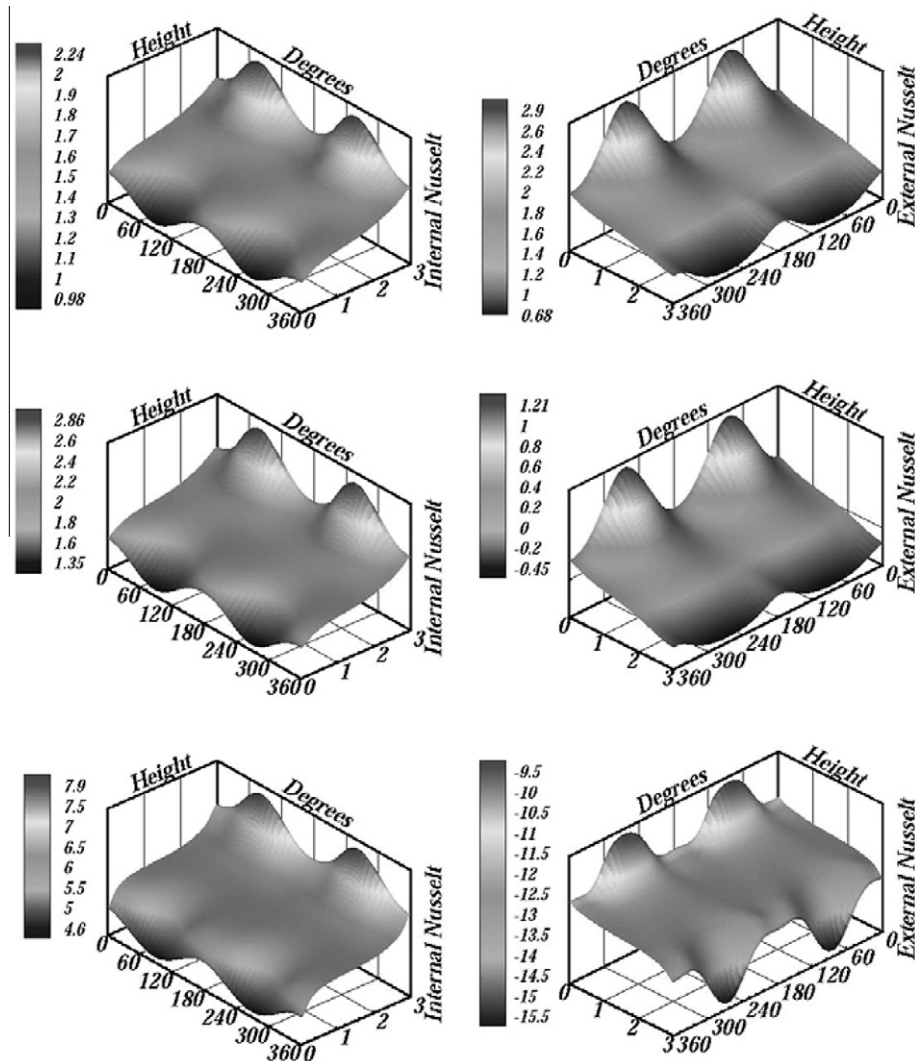


Fig. 14. Local Nusselt number at the inner (left) and outer (right) walls for $Ha = 100$, $Ra_e = 10^4$; $Ra_i = 0$ (top), $Ra_i = 10^4$ (middle), $Ra_i = 10^5$ (bottom).

decreases on the external cylindrical wall because the volumetric heat sources create a second region (very close to the external wall) where the fluid temperature is almost equal to that of the wall. This was demonstrated in Fig. 6 where the time and azimuthally averaged temperature distribution for the hydrodynamic case ($Ha = 0$) and $Ra_e = Ra_i = 10^4$ was presented. As a consequence, the temperature gradients at the outer wall become smoother, resulting to heat transfer reduction. This is shown in Fig. 12 where the time-variation of the average Nusselt number on the inner and outer walls is presented for the hydrodynamic case and for $Ra_e = Ra_i = 10^3, 10^4$ and 10^5 (i.e. $S = 1$). It must be noted that similar results have been presented by Acharya and Goldstein [14] for the natural convection in the volumetrically heated square cavity.

When the magnetic field is imposed, significant effects on the heat transfer mechanism are observed. The fluid is retarded due to the action of the Lorentz force and, thus, convective heat transfer decreases in most cases. More specifically, in the absence of volumetric heating a decrease of the Nusselt number occurs on both walls and, for large values of the Hartmann number heat transfer occurs mainly by conduction. This is demonstrated in Fig. 13 where the time-variation of the average Nusselt number on the inner and outer cylindrical walls is presented for the cases $Ra_i = 0, Ra_e = 10^4$ and $Ha = 25, 50$ and 100 . In addition, the fact that the increase of the magnetic field results to more intense motion of the fluid near the 90° and 270° planes (due to the formation of wider Roberts layers) leads to an analogous heat transfer behavior. More specifically, the Nusselt number is higher near the cylindrical walls parallel to the direction of the magnetic field where the fluid velocities are higher. This is confirmed in Fig. 14 where the local Nusselt number on the inner and the outer cylindrical walls is presented for $Ha = 100, Ra_e = 10^4$ and for $Ra_i = 0, 10^4$ and 10^5 (i.e. without or with internal heating).

5. Conclusions

The combined effect of a horizontal magnetic field and volumetric heating on the natural convection flow and heat transfer of a low Prandtl number fluid in a vertical annulus was studied. Direct numerical simulations were performed for the range of external Rayleigh numbers, $Ra_e = 10^3$ to 10^5 , internal Rayleigh numbers, $Ra_i = 0$ to 10^7 , and for Hartmann numbers, $Ha = 0$ to 100 . For the low Prandtl number ($Pr = 0.0321$) fluid considered here, the flow in the pure hydrodynamic case is turbulent for $Ra_e \geq 10^4$. As the magnetic field increases the flow becomes less turbulent and, for large enough Hartmann numbers ($Ha \geq 75$), it becomes laminar. The magnetic field causes loss of axisymmetry due to the development of Hartmann and Roberts layers near the walls normal and parallel to it, respectively. The flow is damped more in both layers but inside the Hartmann layers the reduction is larger than in the Roberts layers.

The volumetric heating increases the local temperature of the fluid resulting in significant changes of the flow pattern, depending on the ratio of the internal-to-external Rayleigh numbers, $S = Ra_i/Ra_e$. More specifically, for the case of $S = 1$, a second region (very close to the external wall) develops where the temperature becomes almost equal to the maximum value at the external wall. For higher values of S , this region moves towards the middle of the annular gap and the local fluid temperature increases to values exceeding that at the external wall. This leads to the creation of two convection currents because the fluid ascends near the core region of higher temperature and descends close to the walls that are now colder.

Heat transfer increases with increasing external Rayleigh number, resulting to an increase of the average Nusselt number on the walls. An almost similar behaviour is observed when the internal Rayleigh number is increased. However, for the cases when Ra_e and Ra_i are of the same magnitude, the average Nusselt number decreases on the external wall. The presence of the magnetic field results in reduction of convection heat transfer in most cases. This reduction is lower in the 90° and 270° directions, where the Roberts layers form, than at 0° and 180° where the Hartmann layers develop.

Acknowledgments

This work was performed in the framework of the Association EURATOM–Hellenic Republic and is supported by the European Commission within the Fusion Program. IES is thankful for a fellowship from the Association. The content of this publication is the sole responsibility of the authors and it does not necessarily represent the views of the Commission or its services.

References

- [1] I.E. Sarris, S.C. Kakarantzas, A.P. Grecos, N.S. Vlachos, MHD natural convection in a laterally and volumetrically heated square cavity, *Int. J. Heat Mass Transfer* 48 (2005) 3443–3453.
- [2] S.C. Kakarantzas, A.P. Grecos, N.S. Vlachos, I.E. Sarris, B. Knaepen, D. Carati, Direct numerical simulation of a heat removal configuration for fusion blankets, *Energy Convers. Manag.* 48 (2007) 2775–2783.
- [3] S.C. Kakarantzas, I.E. Sarris, A.P. Grecos, N.S. Vlachos, DNS simulation of liquid metal flow in annuli under the effect of a magnetic field and volumetric heating, in: Sixth International Symposium on Turbulence, Heat and Mass Transfer, Rome, 14–18 September, 2009, pp. 993–996.
- [4] F.C. Li, T. Kunugi, A. Serizawa, MHD effect on flow structures and heat transfer characteristics of liquid metal – gas annular flow in a vertical pipe, *Int. J. Heat Mass Transfer* 48 (2005) 2571–2581.
- [5] A. Serizawa, T. Ida, O. Takahashi, I. Michiyoshi, MHD effect of NaK–Nitrogen two phase flow and heat transfer in a vertical round tube, *Int. J. Multiphase Flow* 16 (1990) 761–788.
- [6] N. Uda, M. Hayase, T. Chikaoka, S. Inoue, H. Horiike, K. Miyazaki, Natural convective heat transfer of Lithium under magnetic field, *Fusion Eng. Design* 51–52 (2000) 93–898.
- [7] I.E. Sarris, G.K. Zikos, A.P. Grecos, N.S. Vlachos, On the limits of validity of the low magnetic Reynolds number approximation in MHD natural convection heat transfer, *Numer. Heat Transfer: Part B – Fundam.* 50 (2006) 157–180.
- [8] R. Verzicco, P. Orlandi, A finite-difference scheme for three-dimensional incompressible flow in cylindrical coordinates, *J. Comput. Phys.* 123 (1996) 402–414.
- [9] G. Grötzbach, Spatial resolution requirements for direct numerical simulation of the Rayleigh–Bernard convection, *J. Comput. Phys.* 49 (1983) 241–264.
- [10] J.M. Aurnou, P.L. Olson, Experiments on Rayleigh–Bernard convection, magnetoconvection and rotating magnetoconvection in liquid Gallium, *J. Fluid Mech.* 430 (2001) 283–307.
- [11] S.C. Kakarantzas, I.E. Sarris, A.P. Grecos, N.S. Vlachos, Magneto-hydrodynamic natural convection in a sinusoidal upper heated cylindrical cavity, *Int. J. Heat Mass Transfer* 52 (2009) 250–259.
- [12] I.E. Sarris, I. Lekakis, N.S. Vlachos, Natural convection in a 2D enclosure with sinusoidal upper wall temperature, *Numer. Heat Transfer Part A* 42 (2002) 513–530.
- [13] C. Karcher, Y. Kolesnikov, O. Andreev, A. Thess, Natural convection in a liquid metal heated from above and influenced by a magnetic field, *Eur. J. Mech. – B/Fluids* 21 (16) (2002) 75–90.
- [14] S. Acharya, R.J. Goldstein, Natural convection in an externally heated vertical or inclined square box containing internal energy sources, *ASME J. Heat Transfer* 16 (1983) 855–866.
- [15] L. Todd, Hartmann flow in an annular channel, *J. Fluid Mech.* 28 (1967) 371–384.
- [16] P.A. Davidson, *An Introduction to Magnetohydrodynamics*, Cambridge Univ. Press, Cambridge, 2001.
- [17] A. Shercliff, The flow of conducting fluids in circular pipes under transverse magnetic fields, *J. Fluid Mech.* 1 (1956) 644–666.
- [18] A. Shercliff, Magnetohydrodynamic pipe flow, Part 2. High Hartmann number, *J. Fluid Mech.* 13 (1962) 513–518.
- [19] S. Vantighem, X. Albets-Chico, B. Knaepen, The velocity profile of laminar MHD flows in circular conducting pipes, *Theor. Comput. Fluid Dyn.* 23 (2009) 525–533.
- [20] P.H. Roberts, Singularities of Hartmann layers, *Proc. Roy. Soc. London* 300 (1967) 94–107.